31st Annual International Conference of the IEEE EMBS
Minneapolis, Minnesota, USA, September 2-6, 2009

Evaluation of spatial interpolation strategies for the removal of comb-structure in fiber-optic images

Stephan Rupp and Christian Winter and Matthias Elter

Abstract— **Modern techniques for medical diagnosis and therapy in minimal invasive surgery scenarios as well as industrial inspection make considerable use of flexible, fiber-optic endoscopes in order to gain visual access to holes, hollows, antrums and cavities that are difficult to enter and examine. Unfortunately, fiber-optic endoscopes exhibit artifacts in the images that hinder or at worst prevent fundamental image analysis techniques. The dark comb-like artifacts originate from the opaque cladding layer surrounding each single fiber in the image conductor. Although the removal of comb structure is crucial for fiber-optic image analysis, literature covers only a few approaches. Those are based on Fourier analysis and make use of spectral masking or they operate in the spatial domain and rely on interpolation. In this paper, we concentrate on the latter type and introduce interpolation concepts known from related disciplines to the task of comb structure removal. For a quantitative evaluation, we perform experiments with real images as well as with bivariate test functions and rate an algorithm's performance in terms of the normalized root mean square error - a quality metric that it is most commonly used in signal processing for this purpose. Hence, this paper counters the fact that literature lacks an objective performance comparison of the state-of-the-art interpolation based approaches for this type of application.**

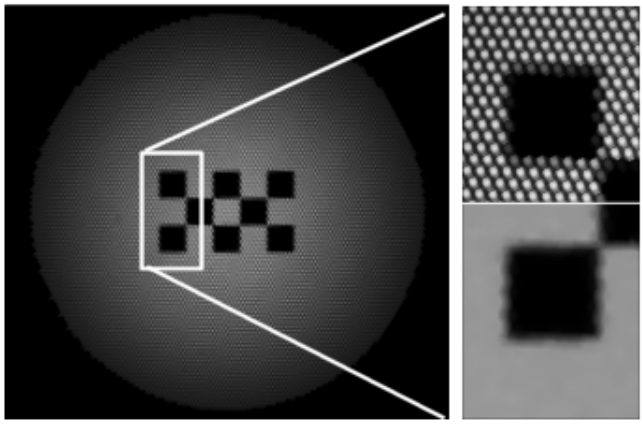

Fig. 1. Image of a small checkerboard being viewed through a flexible endoscope along with a magnified region showing the typical comb structure (top) and a comb-free version obtained by interpolation as described in [3] (bottom).

I. INTRODUCTION

Minimally invasive surgery (MIS) is the most important revolution in surgical technique since the early 1900s [1]. This type of surgery is performed through several small incisions or puncture sites. Typically, rigid or flexible endoscope(s) and surgical instruments are passed through these small entry points. The endoscope(s) enables the surgeon to view the problem area without having to disrupt soft tissue to a large extent. Consequently, MIS is increasingly popular because it reduces operation time, minimizes patient trauma, speeds up recovery time, and saves money - benefiting surgeon and patient [2]. Due to this, endoscopy can legitimately be considered as one of the key technologies for modern medical diagnosis and therapy. In some cases the size of the entry points or the complexity of the scene itself forbids the use of rigid lens-based endoscopes and tip chip videoscopes so that the physician has to resort to flexible, fiber-optic endoscopes. These endoscopes feature a bendable image conductor with a limited number of coated glass or quartz fibers. Each of its optical fibers consists of a core surrounded by a opaque cladding layer. It is this physical layout that leads to dark comb-like imaging artifacts, the so-called comb structure (see Fig.1). Unfortunately, this structure is likely to hinder or even anticipate an appropriate image analysis, hence it needs to be removed in order to apply common image analysis or image processing techniques.

Literature discusses several methods that claim to be able to remove these structures while preserving the image content. These methods either work in the Fourier domain such as low pass filtering [4] and adaptive spectral masking [5] or they operate in the spatial domain and interpolate the cladding areas from pixels containing fiber-optic content. Elter et. al. [3] propose a method that first extracts the fiber center positions with subpixel accuracy and subsequently resamples the image content from the intensities at these positions by interpolation. Unfortunately, neither [3] nor any other publications provide a performance assessment or take other interpolation strategies into consideration. At best, only [6] provides a comparison of a spatial interpolation-based method with a fourier domain method. However, the evaluation focusses on the accuracy of feature extractors for camera calibration from fiber-optic views. It does not address the accuracies of interpolation-based comb-structure removal methods.

In this work, we try to improve these shortcomings and transfer interpolation schemes from related disciplines such as geology, geography, meteorology and computer graphics to the application of comb structure removal. For a quantitative performance assessment, we make use of a normalized version of the commonly used root-mean-square error.

Stephan Rupp, Christian Winter and Matthias Elter are with the Image Processing and Medical Engineering Department, Fraunhofer-Institute IIS, 91058 Erlangen, Germany {rupp,wnt,elt}@iis.fraunhofer.de

II. METHODS

The algorithms presented in this work interpolate the intensities at cladding pixels from the intensities at nearby fiber centers. Consequently, they share the requirement that the (sub)pixel precise center positions of all N_{Fiber} fibers need to be known beforehand. For this, an image of a homogenous bright white scene (i.e. a sheet of paper) is taken and analyzed yielding the (sub)pixel precise location of each fiber. There are many possible ways for a proper extraction of these locations. However, we refer to the original paper [3] that elaborately describes a convenient method.

For the remainder we call the fiber center positions $\mathbf{p}_k$ *stencils* and assume that they have been arranged in a set $\mathbf{S} = \{\mathbf{p}_k : \mathbf{p}_k = (x_k, y_k) \in \mathbf{R}^2, k = 0, \ldots, N_{Fiber} - 1\}$. For a given fiber-optic image I, the task of resampling a comb structure free image $\hat{I}$ can be interpreted as a surface interpolation problem in which we have data values $I_k = I(\mathbf{p}_k)$ defined at the position $\mathbf{p}_k$ contained in the set $\mathbf{S}$. Then, we seek to find a surface $\hat{I}(x, y)$ which takes on the value $\hat{I}_k = I_k$ at the stencils $\mathbf{p}_k$ for $\mathbf{p}_k \in \mathbf{S}$ and provide good approximations $\hat{I}_k$ at non-stencil positions $\mathbf{p}_k \notin \mathbf{S}$. The approximations $\hat{I}_k$ are then the replacements for the intensities at the cladding areas.

The different interpolation methods can be classified with respect to their dependency on local differential properties of the underlying function $\hat{I}(x, y)$, such as first order directional derivatives $\partial_k = \nabla\hat{I}(\mathbf{p}_k)$ at stencils $\mathbf{p}_k$. An alternative approach classifies into global methods, in which each interpolated value is influenced by the values at *all* stencils, and local methods, in which the new value is calculated from nearby stencils only. However, due to the great amount of $N_{Fiber} \in [3000, \ldots, 50000]$ fibers (stencils) in a flexibile endoscope, global methods such as inverse distance weighting [7] or radial basis functions methods [8] will hardly be feasible due to their computational complexity. Consequently, we are forced to apply local methods only and thus resort to the first classification scheme. Due to the fact, that some of the methods rely on a planar partitioning of the stencil set $\mathbf{S}$, a triangulation of $\mathbf{S}$ will be denoted by $\Delta_{\mathbf{S}}$.

A. Local differential independent methods

Data independent methods do not require local differential properties of the underlying function $\hat{I}(x, y)$ in order to derive the value for a query point $\mathbf{q} = (x_q, y_q) \notin \mathbf{S}$. Instead, the intensity $\hat{I}(\mathbf{q})$ is a convex combination of the intensities at the stencils $\mathbf{p}$ in the neighborhood $\mathcal{N}(\mathbf{q})$ of $\mathbf{q}$:

$$\hat{I}(\mathbf{q}) = \sum_{\mathbf{p}\in\mathcal{N}(\mathbf{q})} \omega(\mathbf{p}) I(\mathbf{p}) \ . \tag{1}$$

1) Natural neighbor interpolation (NNI): In natural neighbor interpolation, the neighborhood $\mathcal{N}(\mathbf{q})$ is defined by the set of *natural neighbors* and the weights $\omega(\mathbf{p})$ are given by the *natural neighbor coordinates*. Natural neighbors and their associated coordinates have been introduced by Sibson [9] to interpolate multivariate scattered data. Given a subset of stencils $\mathbf{S}_{\subset} \subseteq \mathbf{S}$, the natural neighbor coordinates associated to $\mathbf{S}_{\subset}$ are defined from the Voronoi diagram $\bar{\Delta}_{\mathbf{S}_{\subset}}$ of $\mathbf{S}_{\subset}$. When simulating the insertion of a query point $\mathbf{q}$ into $\bar{\Delta}_{\mathbf{S}_{\subset}}$, the potential Voronoi cell of $\mathbf{q}$ chops off some parts from the existing cells. Let $A(\mathbf{q})$ denote the area of the potential Voronoi cell of $\mathbf{q}$ and $A_{\mathbf{p}}(\mathbf{q})$ denote the area of the sub-cell that would be stolen from the cell of the stencil $\mathbf{p}$ by the cell of query point $\mathbf{q}$. The natural neighbor coordinate of $\mathbf{q}$ with respect to the stencil $\mathbf{p} \in \mathbf{S}_{\subset}$ is defined by the ratio of the stolen area $A(\mathbf{p})$ and the area of the new cell $A(\mathbf{q})$. Hence, the interpolation is carried out by

$$\hat{I}(\mathbf{q}) = \sum_{\mathbf{p}\in\mathcal{N}(\mathbf{q})} \frac{A(\mathbf{p})}{A(\mathbf{q})} I(\mathbf{p}) \ . \tag{2}$$

This kind of interpolation results in a C^1 continuous surface $\hat{I}(x, y)$ except at the stencils $\mathbf{p}_k$.

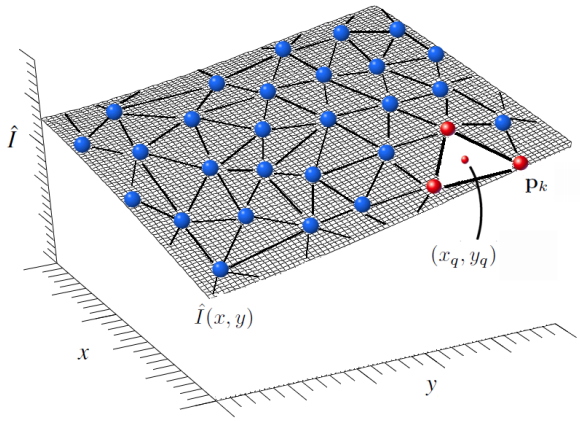

Fig. 2. Resampling of comb-structure free images interpreted as surface interpolation problem. Since only the fiber centers $\mathbf{p}_k$ (represented by the spheres) obtain valid intensity information $\hat{I}(\mathbf{p}_k)$, missing intensities (i.e. at cladding positions (x_q, y_q)) have to be interpolated from the set of fiber centers $\mathbf{S}$. Hence, a comb-structure free image is interpreted as a surface $\hat{I}(x, y)$ that has been reconstructed from the intensities at $\mathbf{p}_k \in \mathbf{S}$.

2) Linear or barycentric interpolation (LI): In contrast to the natural neighbor interpolation that requires a Delaunay triangulation, the piecewise linear interpolation scheme operates on an arbitrary triangulation $\Delta_{\mathbf{S}}$ of $\mathbf{S}$. The surface recovered by this method is C^0 continuous with discontinuities at the triangle boundaries. For an arbitrary query point $\mathbf{q} = (x_{\mathrm{q}}, y_{\mathrm{q}})$ let the enclosing triangle be defined by the three stencils $\mathbf{p}_i = (x_i, y_i), i = 1, \ldots, 3$ with the intensities $I(\mathbf{p}_i)$. Then, the intensity of $\mathbf{q}$ is given by:

$$\hat{I}(\mathbf{q}) = \omega(\mathbf{p}_1) I(\mathbf{p}_1) + \omega(\mathbf{p}_2) I(\mathbf{p}_2) + \omega(\mathbf{p}_3) I(\mathbf{p}_3) \tag{3}$$

with

$$\begin{pmatrix} \omega(\mathbf{p}_1) \\ \omega(\mathbf{p}_2) \\ \omega(\mathbf{p}_3) \end{pmatrix} = \begin{pmatrix} x_1 & x_2 & x_3 \\ y_1 & y_2 & y_3 \\ 1 & 1 & 1 \end{pmatrix}^{-1} \begin{pmatrix} x_{\mathrm{q}} \\ y_{\mathrm{q}} \\ 1 \end{pmatrix} \ . \tag{4}$$

The weights $\omega(\mathbf{p}_k)$ are known as the *barycentric coordinates* of the triangle and they are independent of the intensity values at the stencils $\mathbf{p}_k$.

TABLE I

NORMALIZED RMS ERRORS BETWEEN THE TEST FUNCTIONS AND THEIR RECONSTRUCTION FROM THE SUBPIXEL PRECISE STENCIL SET

	f_1	f_2	f_3	f_4	f_5	f_6
LI	3.81e-6	1.55-5	5.05e-4	2.20e-4	1.66e-4	2.93e-3
NNI	6.50e-6	8.87e-6	4.51e-4	3.35e-4	2.01e-4	2.88e-3
QI	2.80e-6	5.18e-5	4.30e-4	4.00e-4	4.35e-5	**1.03e-3**
NNI[1]	**2.79e-6**	**6.73e-6**	**8.47e-5**	**2.87e-6**	5.53e-6	3.04e-3
BBI	2.91e-6	8.08e-6	1.30e-4	3.47e-5	**3.71e-6**	3.02e-3

TABLE II

DIFFERENCES OF NRMS ERRORS BETWEEN THE INTERPOLATION FROM SUBPIXEL PRECISE AND PIXEL PRECISE STENCILS.

	f_1	f_2	f_3	f_4	f_5	f_6
LI	-5.66e-6	7.17e-6	1.75-04	-4.21e-4	-3.20e-5	1.44e-3
NNI	4.02e-6	-5.86e-6	1.13e-4	-2.62e-4	-2.69e-4	1.57e-3
QI	2.64e-6	-1.28e-5	-1.17e-4	-2.26e-5	-1.05e-5	4.28e-4
NNI[1]	1.52e-6	2.37e-6	-1.06e-4	-1.54e-4	4.81e-6	1.53e-3
BBI	2.53e-6	2.12e-6	-6.70e-5	-9.60e-5	3.39e-6	1.51e-3

B. Local differential dependent methods

In contrast to the former class of interpolation methods, methods subsumed in this category require the knowledge of differential quantities. However, due to the fact that these quantities are unknown, they have first to be estimated from the intensities at the stencils. Consequently, they have to be re-estimated, every time the data at the stencils changes. Suitable methods for the estimation of local differential quantities can be found in [10], [11], [12].

1) C^1 natural neighbor interpolation (NNI[1]): In [9], Sibson describes an interpolation scheme, that results in a C^1 surface $\hat{I}(x,y)$. The method requires the function gradients $\nabla\hat{I}(\mathbf{p}_k)$ to be known or estimated for all stencils $\mathbf{p}_k$. Then, for a query point $\mathbf{q}$, the intensity $\hat{I}(\mathbf{q})$ is given by:

$$\hat{I}(\mathbf{q}) = \frac{\alpha(\mathbf{q})\sum\omega(\mathbf{p})I(\mathbf{p}) + \beta(\mathbf{q})\xi(\mathbf{q})}{\alpha(\mathbf{q}) + \beta(\mathbf{q})} \quad \text{with} \qquad (5)$$

$$\alpha(\mathbf{q}) = \frac{\beta(\mathbf{q})}{\sum\frac{\omega(\mathbf{p})}{||\mathbf{q}-\mathbf{p}||}} \ , \ \beta(\mathbf{q}) = \sum\omega(\mathbf{p})||\mathbf{q}-\mathbf{p}||^2 \qquad (6)$$

and

$$\xi(\mathbf{q}) = \frac{\sum\frac{\omega(\mathbf{p})}{||\mathbf{q}-\mathbf{p}||}I(\mathbf{p}) + \nabla\hat{I}(\mathbf{p})^T(\mathbf{q}-\mathbf{p})}{\sum\frac{\omega(\mathbf{p})}{||\mathbf{q}-\mathbf{p}||}} \ . \qquad (7)$$

As in Sec.II-A.1, $\omega(\mathbf{p})$ denotes the natural neighbor coordinate of the stencil $\mathbf{p}$ and the sum in the above equations is with respect to all stencils $\mathbf{p}$ in the neighborhood $\mathcal{N}(\mathbf{q})$ of the query point $\mathbf{q}$.

2) Quadratic interpolation (QI): With knowledge of the function gradients $\nabla\hat{I}(\mathbf{p}_k)$

$$\hat{I}(\mathbf{q}) = \sum_{\mathbf{p}\in\mathcal{N}(\mathbf{q})}\omega(\mathbf{p})\left(I(\mathbf{p}) + \frac{1}{2}\nabla\hat{I}(\mathbf{p})^T(\mathbf{q}-\mathbf{p})\right) \qquad (8)$$

yields an interpolant that is not C^1 continuous in general. However, it reproduces quadratic functions exactly.

3) Bernstein-Bezier interpolation (BBI): Farin [13] extended Sibson's work and realizes a C^1 continuous interpolant by embedding natural neighbor coordinates in the Bernstein-Bezier representation of a cubic simplex. Thus, the interpolation value of a query point $\mathbf{q}$ is given by the evaluation of the cubic polynomial defined on the triangle $\mathbf{p}_i, i = 1,...,3$ containing the query point $\mathbf{q}$. In order to create a piecewise C^1-continuous interpolation surface $\hat{I}(x,y)$, the method requires the stencils' intensities $I(\mathbf{p}_i)$ of the triangle and the gradients $\nabla\hat{I}(\mathbf{p}_i)$ as well as the normal derivative at the midpoint of each of the three triangle edges in order to ensure that the normal slope matches across triangle boundaries. Then, the aim is to impose these 12 constraints on the cubic polynomial defined on the triangle. Since a bivariate cubic polynomial is determined by only ten coefficients

$$f(x,y) = \sum_{i,j}a_{ij}x^iy^j \ , \quad i,j\in[0,3] \qquad (9)$$

it can only satisfy ten constraints. However, a subdivision of the triangle into subtriangles yields more degrees of freedom and thus allows for satisfying the constraints and solving for the polynomial coefficients. Details on this rather complex algorithm can be found in the original publication [13].

III. EXPERIMENTS AND RESULTS

In this section, we present the evaluation of the different interpolation schemes outlined above. For this, we extract the fiber centers for a flexible glass fiber endoscope with 20000 fibers. The subpixel precise positions are extracted from a 720-by-720 pixel sized white image according to [3]. This stencil set is denoted as $\mathbf{S}$. Analogously, the set $\mathbf{S}_\mathrm{p}$ refers to the same fiber center locations, but in pixel precision only.

A. Test data and quality measure

For the stencil sets, we performed experiments with real images as well as with bivariate test functions. However, we present only the results for the test functions due to space limitations. Certainly, this restriction will not bias the conclusions. The test functions $f_i(x,y), i = 1,...,5$ are taken from [14], because they are commonly used for an evaluation of scattered data interpolation methods. In addition, we extend the set by a checkerboard with two black and two white patches since such patterns are frequently used for sensor calibration:

$$f_6(x,y) = \begin{cases} 1.0 & (\frac{1}{2}\le x,y\le 1)\vee(1\le x,y\le\frac{3}{2}) \\ 0.0 & \text{else} \end{cases} \qquad (10)$$

For a quantitative evaluation, we make use of the normalized root mean square error (nRMS). For each test function $f_i(x,y)$, we first sample data points at the stencils $\mathbf{p}_k$ of a given set $\mathbf{S}$ or $\mathbf{S}_\mathrm{p}$ and apply an interpolation method in order to obtain a reconstruction $\hat{I}(x,y)$ of $f_i(x,y)$. The domain $[0,W-1]\times[0,H-1]$ of $f_i(x,y)$ and $\hat{I}(x,y)$ is defined by the dimension of the white image. By nature, the stencils are irregularly distributed in the domain. In this particular case

they make up 6.5% of the points in the domain:

$$\mathrm{RMS} = \sqrt{\frac{\sum_{x=0}^{W-1}\sum_{y=0}^{H-1}\left(f(x,y)-\hat{I}(x,y)\right)^2}{WH}} \ . \quad (11)$$

In order to ease up the comparison of the results for different functions $f_i(x,y)$, we normalize the RMS by dividing the range of observed values over the domain according to [15], yielding the *normalized root mean square*:

$$\mathrm{nRMS} = \mathrm{RMS}/(\max f_i(x,y) - \min f_i(x,y)) \ . \quad (12)$$

In order to get an impression of the resulting numbers, let us consider commonly used gray scale images with 8-bit. Then a normalized value of $1/256 \approx$ 3.9e-3 equals the difference of one intensity step in the gray scale.

B. Results

Tab.I exhibits the normalized RMS of the algorithms for the stencil set $\mathbf{S}$. The smaller the value is, the better the interpolation method reconstructs the original data. It is shown that the algorithms perform comparably across the set of test functions $f_1, \ldots, f_5$ with one exception. This is due to the sharp edges in the checkerboard modelled by f_6. It is clear that all algorithms suffer from accuaracy imprecisions in this case, because they all share the problem to approximate discontinuities in the underlying function with (piecewise) continuous functions. Consequently, the last column exhibits comparably high errors.

Apart from that, the results shown in Tab.I are indifferent, because the nRMS values are mostly of comparable order for both categories of algorithms. However, algorithms exploiting local differential properties result in slightly lower errors, with the C^1 continuous natural neighbor interpolation (NNI[1]) yielding the best results. Indeed, this comes at the price of higher computational complexity, because the weights $\omega(\mathbf{q}_k)$ have to be re-estimated for every change of the values at the stencil $\mathbf{q}_k$. In contrast, for the linear method (LI) as well as for the natural neighbor interpolation (NNI) method the weights need to be calculated just once, due to the fact that they are independent of the values at the stencils. Hence, it is appropriate to pre-calculate a look-up table that maps a pixel position (x,y) to the stencil positions $\mathbf{p}_k$ and the associated weights $\omega(\mathbf{p}_k)$. By this, interpolation can be significantly accelerated enabling real-time processing of image streams. As a matter of fact, local differential dependent methods can be accelerated when taking advantage of modern graphics cards. Thus, fast processing is feasible in this class, too. However, this is not as straight forward as calculating a lookup table and far beyond the scope of this paper.

Finally, Tab. II shows the differences of the normalized RMS errors when interpolating from the set $\mathbf{S}$ and its pixel-precise counterparts $\mathbf{S}_\mathrm{p}$. For a given function and interpolation method, a positive value indicates that the interpolation from $\mathbf{S}$ yielded a lower normalized RMS than the interpolation from $\mathbf{S}_\mathrm{p}$. The table's values show arbitrarily flipping signs indicating that - in the context of comb structure removal - subpixel precise stencils do not guarantee better interpolation accuracies and thus do not provide a benefit at all.

IV. CONCLUSIONS

In this paper we presented an evaluation of interpolation strategies for use in spatial comb structure removal algorithms. The results have shown that algorithms exploiting local differential properties are only slightly superior in terms of reconstruction accuarcy, but feature high computational complexity. Hence, such algorithms can be a good choice, if the smoothness and continuity of the reconstructed image is of particular interest, while execution time is less important. In any other case, linear interpolation or natural neighbor interpolation seems to be an advisable choice, because they yield comparable results with less complexity. Additionally, it is fairly easy to accelerate such method with a lookup table. Finally, it has been shown that at least in this study the use of subpixel precise fiber center locations does not result in improved reconstruction accuracies as possibly expected.

REFERENCES

[1] A. Darzi and S. Mackay, "Recent advances in minimal access surgery," *British Medical Journal*, vol. 324, pp. 31–34, 2002.

[2] R. M. Jager and S. D. Wexner, *Laparoscopic Colorectal Surgery*, Churchill Livingstone, 1996.

[3] M. Elter, S. Rupp, and C. Winter, "Physically motivated reconstruction of fiberscopic images," in *Proceedings of 18th International Conference on Pattern Recognition*, 2006, vol. 3, pp. 599–602.

[4] M.M. Dickens, D.J. Bornhop, and S. Mitra, "Removal of optical fiber interference in color micro-endoscopic images," *Proceedings of 11th IEEE Symposium on Computer-Based Medical Systems*, pp. 246–251, June 1998.

[5] C. Winter, S. Rupp, M. Elter, C. Münzenmayer, H. Gerhäuser, and T. Wittenberg, "Automatic adaptive enhancement for images obtained with fiberscopic endoscopes," *IEEE Transactions on Biomedical Engineering*, vol. 53, pp. 2035–2046, October 2006.

[6] Stephan Rupp, Christian Winter, and Matthias Elter, "Improving the accuracy of feature extraction for flexible endoscope calibration by spatial super resolution," in *29th Annual International Conference of the IEEE Engineering in Medicine and Biology Society*. August 2007, pp. 6565–71, IOP Publishing, Bristol.

[7] D. Shepard, "A two-dimensional interpolation function for irregularly spaced data," in *Proceedings of the 23rd ACM National Conference*, 1968, pp. 517–524.

[8] R. L. Hardy, "Multiquadric equations of topography and other irregular surfaces," *J. Geophys. Res.*, vol. 76, pp. 1905–1915, 1971.

[9] R. Sibson, "A brief description of natural neighbour interpolation," *Interpreting Multivariate Data, John Wiley and Sons Ltd.*, pp. 21–36, 1981.

[10] S. Stead, "Estimation of gradients from scattered data," *Rocky Mountain Journal of Mathematics*, vol. 14, no. 1, pp. 265–279, 1984.

[11] T. N. T. Goodman, H. B. Said, and L. H. T. Chang, "Local derivative estimation for scattered data interpolation," *Applied Mathematics and Computation*, vol. 68, no. 1, pp. 41 – 50, 1995.

[12] Y. Ooi, L.H.T. Chang, Y.P. Wong, and A.R.M. Piah, "A choice of weights for convex combination methods in estimating partial derivatives," in *CGIV '04: Proceedings of the International Conference on Computer Graphics, Imaging and Visualization*, Washington, DC, USA, 2004, pp. 233–236, IEEE Computer Society.

[13] G. Farin, "Surfaces over dirichlet tessellations," *Computer Aided Geometric Design*, vol. 7, pp. 281–292, 1990.

[14] R. Franke and G. Nielson, "Smooth interpolation of large sets of scattered data," *International Journal for Numerical Methods in Engineering*, vol. 15, pp. 1691 – 1704, 2005.

[15] S. Lee, G. Wolberg, and S. Y. Shin, "Scattered data interpolation with multilevel b-splines," *IEEE Transactions on Visualization and Computer Graphics*, vol. 3, pp. 228–244, 1997.